A Load Estimator-Based Fast Terminal Super-Twisting Control Strategy For Performance Improvement Of Induction Machine System Drive

Donghai Liu

Intelligent Manufacturing College of Guangxi Vocational & Technical College, Nanning City, Guangxi Province, 530226, China

Corresponding author. E-mail: 15177160962@163.com

Received: Jun. 28, 2025; Accepted: Mar. 31, 2026

In this work, a hybrid control strategy derived from the control literature for induction machines is proposed, where a sliding-mode controller paired with an estimator from the same function is incorporated to provide fast, robust speed regulation while minimizing chattering. The controller operates using a fast integral terminal sliding surface that accelerates the convergence rate of tracking error after entering the sliding surface. A new super-twisting reaching law is provided which incorporates an integral term designed to suppress high-frequency switching actions associated with chattering. The estimator that accompanies the controller also implements the same sliding surface coupled with the reaching law to estimate load torque and send the estimate to the controller to improve performance during sudden changes in load or when models are uncertain. Experimental results demonstrate the proposed method successfully (i) reduced convergence time (ii) reduced quaternion-like oscillations (chattering) (iii) improved performance robustness to time-varying load time, and where models were uncertain. From the results, it can be seen that the proposed approach improves chattering substantially (around 7% lower chattering), and convergence times are reduced to approximately 0.15 - 0.25 sec, as opposed to the 0.8 - 0.9 sec convergence times found with the reference. Speed tracking is better, on average, by around 9%, and transient torque errors went down to about 1 - 2 rpm. Overall, it can be said that performance is better when compared to the reference.

Keywords: Induction machine, sliding mode Control, super-twisting, speed, chattering, integral terminal sliding surface, fast convergence.

http://dx.doi.org/10.6180/jase.202609_32.071

1. Introduction

Because of their dependability, power, as well as efficiency, induction machines are widely used in industry. Induction machine speed control is essential for achieving optimum performance, high energy efficiency, and improved process control. In the literature review that follows, some of the techniques employed in induction machine speed control, ranging from conventional to advanced, are described, including scalar control, vector control, direct torque control, and the recent advancements in the application of Artificial Intelligence (AI) in machine control [1, 2].

Scalar control techniques are the simplest methods to regulate the speed of induction machines, primarily voltage and frequency control methods. Of these, Voltage-to-Frequency (V/f) control, with parameters of voltage and frequency, has the widest adoption for induction motor control [3]. By maintaining a consistent voltage-to-frequency ratio, this method effectively prevents saturation and simplifies the process of controlling speed. V/f control performs reliably under steady-state conditions; however, it tends to face difficulties when dealing with dynamic changes and often requires adjustment to maintain adequate torque during transient situations [4]. An

additional scalar approach is slip control. This is when the machine speed is manipulated through the adjustment of slip, which is defined as: synchronous speed - actual rotor speed. The concept of slip is utilized whereby the slip is shortlisted to a desired value by varying the rotor resistance or stator voltage which results in an indirect influence on speed. The dynamic performance in terms of response time of scalar methods is slower than in the vector control methods, ultimately scalar methods are generally unsuitable for applications that require fast dynamic performance [5]. By decoupling the regulation of torque and flux, vector control, known as field-oriented control, represents an advancement over the scalar method [6].

The method allows separate regulation of magnetizing flux and machine torque thereby allowing improved torque and speed control. Vector control modifies the machine currents to a rotating reference frame aligned with the rotor field. This transformation gives direct control over the magnetizing and torque-producing components of the stator current. Due to advances in the field of digital signal processing and microcontroller technology, development of vector control strategies that can carry out the computations required for control in real-time has become possible. Induction machines that are controlled via vector control techniques have a significantly improved dynamic response and are particularly attractive for applications that exhibit variable load and rapid start-stop cycles. There has been a development of a variety of algorithms to improve their vector control performance which includes using Proportional- Integral- Derivative (PID) Controllers [7] and Model Predictive Control (MPC) approaches [8, 9]. Direct Torque Control (DTC) [10] is yet another advanced technique that allows better dynamic performance by directly controlling machine torque and flux. DTC was developed in the early 1990's and uses a hysteresis control approach to torque and flux in order to provide quick response times and greater efficiency. The most important feature of DTC is that it produces high torque generation without utilizing Pulse Width Modulation (PWM) techniques. Rather, DTC employs a switching table to select the correct voltage vector depending on the desired torque and flux level. The design of sliding mode controller based on the DTC concept is one of the most popular methods in the induction machine control [11, 12]. The major advantage of DTC over vector control is its less reliance on complex mathematical models and its ability to provide a faster response to speed and load changes. This characteristic makes DTC highly applicable in systems that require accurate speed and torque control, e.g., industrial automation systems and electric vehicles. Researchers have been consistently refining DTC algorithms to improve its performance under different operating conditions, including the optimization of torque ripple and flux performance [13].

Though traditional control methods generally rely on sensors to provide instantaneous feedback of rotor speed and position, sensorless control strategies are now a viable alternative to reduce system complexity and cost. They estimate the position and speed of the rotor based on measurements of stator voltage and current and thus eliminate the need for physical sensors like encoders [14]. One of the most popular sensorless techniques employs the use of observers like the Luenberger observer [15] or the Extended Kalman Filter (EKF) [16]. These observers rely on mathematical models of machine dynamics to make rotor parameter estimates from electrical quantities. Sensorless control can reach a level of performance equivalent to the performance of sensor - based systems by the fact that these estimates can always be improved upon in real - time. Sensorless control is beginning to be adopted, especially in applications with limited installation space and high cost. Current work in the field is focused on achieving higher accuracy and stability of such estimation techniques so they can be used over extensive operating ranges [17]. The emergence of AI [18] and Machine Learning (ML) [19] have potential implications for many engineered systems, including induction machine control. AI-based strategies leveraging data-driven approaches allow for optimization of machine performance through improved operation. With AI and ML, researchers are developing intelligent control architectures based on neural networks, decision trees, and other ML algorithms, enabling machine systems to learn and adapt under various conditions and improve from prior experiences. One particular class of ML, reinforcement learning, consists of agents learning to modify control parameters in real time by feedback pertaining to the machine system. This degree of adaptability has the potential to outperform conventional fixed-parameter control and adjust to variable loads and operating conditions [20].

Additionally, AI enables predictive maintenance, allowing real-time monitoring of induction machine health and forecasting failures before they occur. AI systems suggest maintenance schedules, detect anomalies, and optimize operational efficiency based on pattern recognition and historical data, thereby reducing operating costs and downtime. Further research has incorporated various control approaches to harness their respective advantages. Hybrid control techniques involve mixing concepts of scalar, vector, DTC, and AI-based techniques to create more effective and timely control systems. For instance, a system may employ vector control for steady-state and switch automatically

to DTC during transient states, optimizing performance according to operating needs at a given time [21, 22]. Another instance of hybrid control includes the fusion of AI algorithms with traditional control, where an AI system is utilized to learn the parameters of a typical controller from real-time data. Such a hybrid can establish a flexible and adaptive framework that learns from historical operating conditions and improves control accuracy over time. Though improvement has been achieved in the evolution of speed control methods for induction machines, their implementation and usage are still cumbersome. Sophistication in techniques such as vector control, DTC, and hybrid approaches may lead to excessive computational loads and the requirement for sophisticated hardware. Additionally, guaranteeing robustness and reliability under varying operating conditions is still an active area of research [23]. Furthermore, the incorporation of AI-based solutions into existing machine control systems must be carried out with caution. Issues of data quality, training of systems, and explainability of AI decisions are problems that require ongoing research and technical development. The evolving landscape of induction machine management is characterized by a trend towards a heightened utilization of digital technology and the integration of intelligent systems. As the demand for energy-efficient solutions persists and advances in semiconductor technology and computing capabilities progress, the future of speed control in induction machines is expected to involve continuous methodological evolution to ensure improved performance and sustainability.

For this purposed, controllers such as Robust Sampled-Data Control for Switched Complex Dynamical Networks [24], Aperiodic Sampled-Data Networked Control Systems [25], neutral descriptor hybrid systems [26] and molding through p-norm stochastic nonlinear systems [27] seem to be proper choices. The standard super-twisting methods had deficiencies involving consistency in chattering during transient behavior and slow convergence speed, along with possible deviations from the reference caused by disturbance, particularly during load variation and machine parameter uncertainty highlighted in the case of induction-machine drives. These deficiencies included: (1) the absence of integral action, which leads to steady-state error, (2) lack of rapid convergence speed with abrupt reference changes, (3) real-time load torque estimation would need to be incorporated into the same sliding surface, and (4) residual switching loss that affects inverter lifetime. The proposed method develops and implements a fast-integral terminal sliding surface, along with an integral-super-twisting reaching law and a sliding family load-torque estimator, to achieve significant decreases in chattering, enhanced convergence speed, disturbance rejection, faster torque-tracking, and use of the same physical sliding surface, and thereby address the described deficiencies in research, based on the combination of the latter, experimentally derived previously.

This paper introduces a hybrid control scheme consisting of a controller and an estimator from the class of sliding mode control to control the speed of an induction machine. The goal is to minimize chattering and improve the convergence rate. A special sliding mode controller is introduced that uses a fast integral terminal sliding surface, which raises the convergence rate for the controller. This scheme significantly increases the convergence rate of the tracking error towards zero after crossing the sliding surface. Besides, a new reaching law with a super-twisting structure and an integral term is employed in this controller to eliminate high-frequency switching terms and thus significantly reduce chattering. The article also presents an estimator belonging to the same class of sliding modes, utilizing the same reaching law and sliding surface as the controller. The purpose of this estimator is to estimate the load torque and provide it to the controller to increase the system's robustness against sudden changes in the load. The main contributions of this study are:

- **Unified fast integral terminal sliding surface:** Introduces a fast integral terminal sliding surface that accelerates convergence and improves tracking accuracy for induction motor control.
- **Integral-super-twisting reaching law:** Combines an integral component with the super-twisting framework to robustly reject disturbances and reduce steady-state error under load variations.
- **Sliding-family load-torque estimator:** Adds a real-time estimator to identify and compensate load-torque dynamics, enhancing torque-tracking robustness.
- **Reduced chattering and improved disturbance rejection:** Demonstrates significant chattering reduction and better handling of high-frequency disturbances and parameter drift.
- **Experimental validation:** Provides experimental results validating performance improvements across step, ramp, and transient maneuvers.
- **Clear research gaps and future directions:** Identifies limitations and outlines avenues for future work, including AI-assisted adaptation and extension to high-power motors.

The remaining parts of the article are categorized as follows: In the second part, induction machine modeling will be presented, and the desired control method consisting of the controller and estimator will be formulated in the third part. The fourth part presents the findings from real-world tests, and the fifth part wraps up the work.

2. Induction machine dynamic equations

The electromagnetic induction concept is the basis for the torque produced by an induction machine or an AC electric machine. In an induction machine, torque is produced by a revolving magnetic field that generates the rotor current. To induce torque, a magnetic field is created using alternating current (AC). The induction machine essentially consists of two most crucial parts: the stator, in which the windings are installed, and the rotor, through which motion is facilitated. Other than these crucial parts, induction machines also consist of required parts such as end bells, bearings, and a machine frame, which provide structural strength and facilitate smooth operation. The rotor's current is generated through electromagnetic induction, allowing the induction machine to function efficiently without the need for brushes or commutators. Such durable and simple design renders induction machines very suitable to widespread application across numerous fields, including industrial machinery, fans, pumps, and numerous others. The fact that they are very reliable and consume low maintenance also makes them very popular. For better understanding, refer to Fig. 1, which is a diagram illustrating the basic structure of a three-phase induction machine and its main elements and layout.

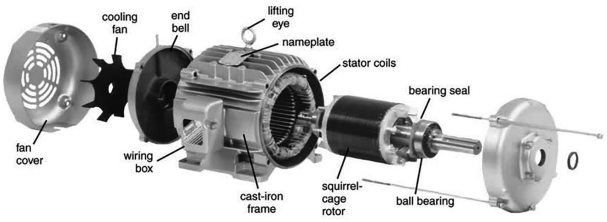

Fig. 1. The structure of induction machine.

The dynamic behavior of stator currents in the dq-frame for an induction machine is outlined as follows [28]:

$$\begin{aligned}\dot{I}_{sd} &= -\frac{r_s L_r^2 + r_r L_m^2}{C L_s L_r^2} I_{sd} + \omega_e I_{sq} + \frac{L_m}{C L_s L_r t_r}\vartheta_r + \frac{V_{sd}}{C L_s} \\ \dot{I}_{sq} &= -\frac{r_s L_r^2 + r_r L_m^2}{C L_s L_r^2} I_{sq} - \omega_e I_{sd} - \frac{L_m}{C L_s L_r}\omega_r \vartheta_r + \frac{V_{sq}}{C L_s}\end{aligned} \tag{1}$$

where:

$$C = 1 - L_m^2 L_s^{-1} L_r^{-1} \tag{2}$$

$$t_r = L_r r_r^{-1} \tag{3}$$

In Eqs. (1) to (3), ω_e is the synchronous angular speed, L_s, L_r, and L_m in that order are the stator inductance, the rotor inductance, as well as the mutual inductance, ϑ_r is the rotor flux, r_s and r_r respectively represent the stator resistances and rotor resistances and I_{sd}, I_{sq}, V_{sd}, and V_{sq} respectively represent the stator currents and the stator voltages in dq-frame. Also, ω_r is the rotor angular velocity and is obtained by following dynamic equation:

$$\dot{\omega}_r = 1.5 n_p L_m \psi_r L_r^{-1} I^{-1} I_{sq} - T_L I^{-1} - c\omega_r I^{-1} \tag{4}$$

where T_L, c, I, and n_p represent the external load torque, the viscous friction coefficient, the rotational inertia, and the pole pairs, respectively. Define $e_\omega = \omega_r - \omega_{\text{ref}}$ where ω_{ref} is the reference rotor angular speed. Assuming $\dot{T}_L \approx 0$ and due to Eq. (4), the following can be obtained:

$$\dot{e}_\omega = 1.5 n_p L_m \vartheta_r L_r^{-1} I^{-1} I_{sq} - T_L I^{-1} - c\omega_r I^{-1} - \dot{\omega}_{ref} \tag{5}$$

$$\ddot{e}_\omega = 1.5 n_p L_m \vartheta_r L_r^{-1} I^{-1} \dot{I}_{sq} - c\dot{\omega}_r I^{-1} - \ddot{\omega}_{ref} \tag{6}$$

3. The structure of induction machine drive system

Fig. 2presents the proposed structure for the induction machine drive system. This design utilizes a super twisting reaching law-based fast integral terminal sliding mode controller (STRL-based FITSMC) to generate the reference current for the q-frame. Additionally, a super twisting reaching law-based fast integral terminal sliding mode estimator is implemented to assess variations in the motor load, adjusting the reference current for the q-frame as needed. Meanwhile, a proportional-integral (PI) controller is employed to generate the voltages in the dq-frame based on current errors.

4. Development of novel controller

First, a fast integral terminal sliding surface is suggested as follows:

$$S = \dot{e}_\omega + c_1 \int |e_\omega(\tau)|^{\frac{b}{a}} \operatorname{sign}\left(e_\omega(\tau)\right) d\tau + c_2 e_\omega, c_1 > 0, c_2 > 0 \tag{7}$$

where a and b are odd numbers. This sliding surface not only reduces the convergence time but also decreases the

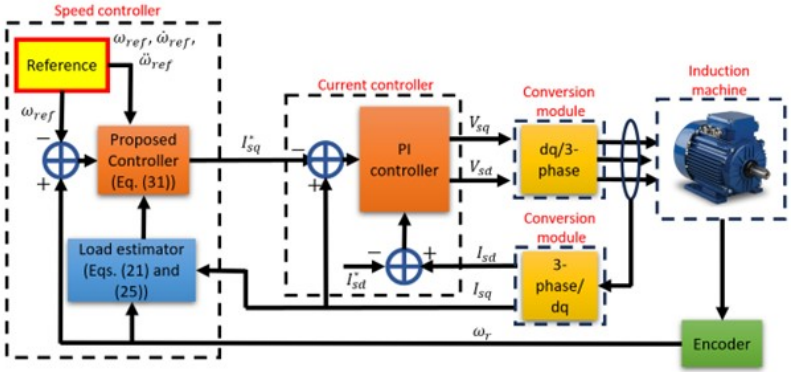

Fig. 2. The structure of suggested controller for induction motor drive system.

steady-state error. A convergence time analysis will be presented next. By setting $S = 0$, the bellow formula can be obtained:

$$S = 0 \Rightarrow \dot{e}_\omega + c_1 \int |e_\omega|^{\frac{b}{a}} \operatorname{sign}(e_\omega)\, dt + c_2 e_\omega = 0 \quad (8)$$

By defining $F = \int |e_\omega| \operatorname{sign}(e_\omega)\, dt$, Eq. (8)is rewritten as:

$$\ddot{F} = -c_1 F^{\frac{b}{a}} - c_2 \dot{F} \Rightarrow \dot{F} d\dot{F} = \left(-c_1 F^{\frac{b}{a}} - c_2 \dot{F}\right) dF \quad (9)$$

By taking the integral of both sides, the following can be attained:

$$\begin{aligned}
&\int_0^{F(t_r)} \dot{F} d\dot{F} = \int_0^{F(t_r)} \left(-c_1 F^{\frac{b}{a}} - c_2 \dot{F}\right) dF \\
&\Rightarrow \int_0^{F(t_r)} -c_2 \dot{F} dF = \int_0^{F(t_r)} \dot{F} d\dot{F} + \int_0^{F(t_r)} c_1 F^{\frac{b}{a}} dF \\
&\Rightarrow \int_0^{F(t_r)} -c_2 \dot{F} dF \times \frac{dt}{dt} = \int_0^{F(t_r)} \dot{F} d\dot{F} + \int_0^{F(t_r)} c_1 F^{\frac{b}{a}} dF \\
&\Rightarrow \int_0^{T} -c_2 \dot{F}^2 \times dt = \int_0^{F(t_r)} \dot{F} d\dot{F} + \int_0^{F(t_r)} c_1 F^{\frac{b}{a}} dF
\end{aligned} \quad (10)$$

where t_r represents the time at which the tracking error reaches the sliding surface and T represents the convergence time. By solving Eq. (10), it can be obtained:

$$\begin{aligned}
\int_0^T c_2 \dot{F}^2 dt &= \frac{\dot{F}^2(t_r)}{2} + \frac{c_1 b F^{\frac{a+b}{b}}(t_r)}{a+b} \\
&= \frac{{e_\omega}^2(t_r)(a+b) + 2c_1 b F^{\frac{a+b}{b}}(t_r)}{2(a+b)}
\end{aligned} \quad (11)$$

Due to Eq. (11), T is obtained as follows:

$$T = \frac{2c_2 {e_\omega}^2(t_r)(a+b)}{{e_\omega}^2(t_r)(a+b) + 2c_1 b F^{\frac{a+b}{b}}(t_r)} \quad (12)$$

The relationship between the sliding surface characteristics and the convergence time is demonstrated by Eq. (12). Therefore, by adjusting these parameters, the desired convergence time can be obtained.

The reference stator current in the q-frame is now suggested to be:

$${I_{sq}}^* = I_{sq,eq} + I_{sq,rl} \quad (13)$$

where $I_{sq,eq}$ signifies to the equivalent part and $I_{sq,rl}$ signifies the reaching law part.

$I_{sq,eq}$ is derived as:

$$\dot{S} = 0 \Rightarrow \ddot{e}_\omega + c_1 e_{\dot{\omega}}^{\frac{b}{a}} \operatorname{sign}(e_\omega) + c_2 \dot{e}_\omega = 0 \quad (14)$$

By substituting Eq. (6) into Eq. (14):

$$\begin{aligned}
&1.5 n_p L_m \varphi_r L_r^{-1} I^{-1} I_{sq,eq} - c\dot{\omega}_r I^{-1} - \ddot{\omega}_{ref} + c_1 e_{\dot{\omega}}^{\frac{b}{a}} \operatorname{sign}(e_\omega) + c_2 \dot{e}_\omega = 0 \\
&\Rightarrow \dot{I}_{sq,eq} = \left(1.5 n_p L_m \varphi_r L_r^{-1} I^{-1}\right)^{-1} \left(c\dot{\omega}_r I^{-1} + \ddot{\omega}_{ref} - c_1 e_{\dot{\omega}}^{\frac{b}{a}} \operatorname{sign}(e_\omega) - c_2 \dot{e}_\omega\right) \\
&\Rightarrow I_{sq,eq} = \int \left(1.5 n_p L_m \varphi_r L_r^{-1} I^{-1}\right)^{-1} \left(c\dot{\omega}_r I^{-1} + \ddot{\omega}_{ref} - c_1 e_{\dot{\omega}}^{\frac{b}{a}} \operatorname{sign}(e_\omega)\right. \\
&\left. - c_2 \dot{e}_\omega\right) dt
\end{aligned} \quad (15)$$

Also, $I_{sq,rl}$ is derived as:

$$I_{sq,rl} = \int \left(1.5 n_p L_m \varphi_r L_r^{-1} I^{-1}\right)^{-1} \left(-\rho_1 |S|^{\frac{1}{2}} \operatorname{sign}(S) - \int \rho_2 \operatorname{sign}(S) dt\right) dt$$
$$, \rho_1 > 0, \rho_2 > 0 \quad (16)$$

Note that Eq. (16) is written based on super twisting reaching law. This reaching law uses fractional power term $\left(|S|^{\frac{1}{2}} \operatorname{sign}(S)\right)$ to smooth the control law. Therefore, the high frequencies arising from the control law (chattering phenomenon) are reduced and the control performance improves. Additionally, the high-frequency noise present in the measurement sensors and the environment is suppressed. As a result, an intrinsic robustness also emerges in the control law.

By summing Eqs. (15) and (16), it can be obtained:

$$I_{sq}^{*}=\left(1.5n_pL_m\varphi_rL_r^{-1}I^{-1}\right)^{-1}\left(\int\left(c\dot{\omega}_rI^{-1}+\ddot{\omega}_{ref}-c_1e_{\omega}^{\frac{b}{a}}\operatorname{sign}\left(e_{\omega}\right)\right.\right.$$
$$\left.\left.-c_2\dot{e}_{\omega}-\rho_1|S|^{\frac{1}{2}}\operatorname{sign}(S)-\int\rho_2\operatorname{sign}(S)dt\right)dt\right) \tag{17}$$

From Eqs. (6), (7) and (17), it can derive:

$$\begin{aligned}\dot{S}&=\ddot{e}_{\omega}+c_1e_{\omega}^{\frac{b}{a}}\operatorname{sign}\left(e_{\omega}\right)+c_2\dot{e}_{\omega}\\&=1.5n_pL_m\varphi_rL_r^{-1}I^{-1}i_{sq}^{*}-c\dot{\omega}_rI^{-1}-\ddot{\omega}_{ref}+c_1e_{\omega}^{\frac{b}{a}}\operatorname{sign}\left(e_{\omega}\right)+c_2\dot{e}_{\omega}\\&=1.5n_pL_m\varphi_rL_r^{-1}I^{-1}\left(1.5n_pL_m\varphi_rL_r^{-1}I^{-1}\right)^{-1}\\&\left(c\dot{\omega}_rI^{-1}+\ddot{\omega}_{ref}-c_1e_{\omega}^{\frac{b}{a}}\operatorname{sign}\left(e_{\omega}\right)-c_2\dot{e}_{\omega}-\rho_1|S|^{\frac{1}{2}}\operatorname{sign}(S)-\right.\\&\left.\int\rho_2\operatorname{sign}(S)dt\right)-c\dot{\omega}_rI^{-1}-\ddot{\omega}_{ref}+c_1e_{\omega}^{\frac{b}{a}}\operatorname{sign}\left(e_{\omega}\right)+c_2\dot{e}_{\omega}\\&=-\rho_1|S|^{\frac{1}{2}}\operatorname{sign}(S)-\int\rho_2\operatorname{sign}(S)dt\end{aligned} \tag{18}$$

Now, the stability analysis is discussed. The Lyapunov function is defined as:

$$V_1=0.5S^2 \tag{19}$$

Based on Eqs. (18) and (19), $\dot{V}_1$ is extended as:

$$\begin{aligned}&\dot{V}_1=S\dot{S}=S\left(-\rho_1|S|^{\frac{1}{2}}\operatorname{sign}(S)-\int\rho_2\operatorname{sign}(S)dt\right)=-\rho_1|S|^{\frac{3}{2}}-\\&S\int\rho_2\operatorname{sign}(S)dt=-\rho_1|S|^{\frac{3}{2}}-\rho_2|S|\int dt\\&=\rho_12^{\frac{3}{4}}V_1^{\frac{3}{4}}-\left(\rho_22^{0.5}\int dt\right)V_1^{\frac{1}{2}}\end{aligned} \tag{20}$$

Due to $\rho_1>0$ and $\rho_2>0$, it is concluded that $\rho_12^{\frac{3}{4}}>0$ and $\rho_22^{0.5}\int dt>0$. Also, powers of V_1 are between zero and one. Therefore, the finite-time stability is satisfied and $S\to 0$ in finite time. The finite-time stability condition depends on two parameters ρ_1 and ρ_2. When these parameters are positive, the finite-time stability condition is satisfied. From Eqs. (7) and (20), increasing the values of ρ_1 and ρ_2 leads to reduce convergence time, but it also raises the chattering in the control law. Consequently, these parameters should be raised from 0 upward until the resulting chattering no longer exceeds the specified limit. When S reaches zero, the tracking error dynamics follows Eq. (8). In Eqs. (9) to (12), it was shown that the tracking error reaches zero in finite time T. Note that the following conditions must be met for the parameters in the Eq. (8) for the tracking error to reach zero: $c_1>0, c_2>0$, and a and b are odd numbers with $0<\frac{b}{a}<1$.

5. Development of novel load estimator

Conventional estimators do not have the ability to simultaneously provide high convergence speed, significantly reduce the chattering level, and reduce the estimation error, and a compromise must always be made between these three. The design of the estimator based on the super-twisting reaching law and the integral sliding surface allows it to reduce the high frequencies caused by chattering, provide finite time stability to increase the convergence speed, and reduce the estimation error due to the presence of the integral term. Furthermore, the proposed estimator establishes a tangible relationship between the parameters, convergence speed, and chattering level to give the reader a better view and choose the desired parameters accordingly.

First, based on Eq. (4), the following estimator is suggested:

$$\begin{aligned}\dot{\widehat{\omega}}_r&=1.5n_pL_m\varphi_rL_r^{-1}I^{-1}i_{sq}-I^{-1}\hat{T}_L-I^{-1}c\omega_r+\alpha_1\Gamma\\\dot{\hat{T}}_L&=\alpha_2\Gamma\end{aligned} \tag{21}$$

where k_1 and k_2 indicates design parameters and Γ indicates the sliding mode function.

Also, $\widehat{\omega}_r$ and $\widehat{T}_L$ respectively indicate the estimation of T_L and the estimation of ω_r. Define $\sigma_1=\omega_r-\widehat{\omega}_r$ and $\sigma_2=T_L-\widehat{T}_L$. According to Eqs. (4) and (21) and assuming $\dot{T}_L=0$, it can be obtained:

$$\dot{\sigma}_1=-I^{-1}\sigma_2-\alpha_1\Gamma \tag{22}$$

$$\dot{\sigma}_2=-\alpha_2\Gamma \tag{23}$$

A fast integral terminal sliding surface is suggested as:

$$R=\dot{\sigma}_1+d_1\int|\sigma_1|^{\frac{q}{p}}\operatorname{sign}\left(\sigma_1\right)dt+d_2\sigma_1, d_1>0, d_2>0 \tag{24}$$

where p and q are odd numbers. Now, Γ is designed as:

$$\begin{aligned}\Gamma=\int\alpha_1^{-1}\left(-I^{-1}\dot{\sigma}_2+d_1\int|\sigma_1|^{\frac{q}{p}}\operatorname{sign}\left(\sigma_1\right)dt+d_2\sigma_1\right.\\\left.+\tau_1|R|^{\frac{1}{2}}\operatorname{sign}(R)+\int\tau_2\operatorname{sign}(R)dt\right)dt, \tau_1>0, \tau_2>0\end{aligned} \tag{25}$$

From Eqs. (22) to (25), it can be derived:

$$\begin{aligned}&\dot{R}=\ddot{\sigma}_1+d_1\sigma_1^{\frac{q}{p}}\operatorname{sign}\left(\sigma_1\right)+d_2\dot{\sigma}_1=-I^{-1}\dot{\sigma}_2-\alpha_1\dot{F}+d_1\sigma_1^{\frac{q}{p}}\operatorname{sign}\left(\sigma_1\right)\\&+d_2\dot{\sigma}_1=-I^{-1}\dot{\sigma}_2-\alpha_1\left(\alpha_1^{-1}\left(-I^{-1}\dot{\sigma}_2+d_1\int|\sigma_1|^{\frac{q}{p}}\operatorname{sign}\left(\sigma_1\right)dt+d_2\sigma_1\right.\right.\\&\left.\left.+\tau_1|R|^{\frac{1}{2}}\operatorname{sign}(R)+\int\tau_2\operatorname{sign}(R)dt\right)\right)+d_1\sigma_1^{\frac{q}{p}}\operatorname{sign}\left(\sigma_1\right)+d_2\dot{\sigma}_1\\&=-\tau_1|R|^{\frac{1}{2}}\operatorname{sign}(R)-\int\tau_2\operatorname{sign}(R)dt\end{aligned} \tag{26}$$

Now, the stability analysis is discussed. The Lyapunov function is defined as:

$$V_2=0.5R^2 \tag{27}$$

According to Eqs. (26) and (27), it is obtained that:

$$\begin{aligned}&\dot{V}_2=R\dot{R}=R\left(-\tau_1|R|^{\frac{1}{2}}\operatorname{sign}(R)-\int\tau_2\operatorname{sign}(R)dt\right)=-\tau_1|R|^{\frac{3}{2}}\\&-R\int\tau_2\operatorname{sign}(R)dt=-\tau_1|R|^{\frac{3}{2}}-\tau_2|R|\int dt-\tau_12^{\frac{3}{4}}V_2^{\frac{3}{4}}-\tau_22^{0.5}\int dtV_2^{\frac{1}{2}}\end{aligned} \tag{28}$$

Due to $\tau_12^{\frac{3}{4}}>0$ and $\tau_22^{0.5}\int dt>0$, the finite-time stability is satisfied. Thus, based on

Eqs. (24) and (28), it is concluded that: $\sigma_1, \dot{\sigma}_1\to 0$. As a result, from Eq. (22), it is obtained that:

$$\Gamma=-\alpha_1^{-1}I^{-1}\sigma_2 \tag{29}$$

By substituting Eq. (29) into Eq. (23), it is obtained that:

$$\dot{\sigma}_2=\alpha_2\alpha_1^{-1}I^{-1}\sigma_2 \tag{30}$$

By solving Eq. (30), it is obtained that: $\sigma_2 = e^{\alpha_2\alpha_1^{-1}I^{-1}t}$. Therefore, if $\alpha_2\alpha_1^{-1} < 0$, then $\sigma_2 \to 0$. By estimating T_L, the reference stator current in q-frame is obtained as follows:

$$I_{sq}^{*} = \left(1.5n_pL_m\varphi_rL_r^{-1}I^{-1}\right)^{-1}\left(\int\left(c\dot{\omega}_rI^{-1} + \ddot{\omega}_{ref} - c_1e_\omega^{\frac{b}{a}}\,\mathrm{sign}\,(e_\omega) - c_2\dot{e}_\omega - \rho_1|S|^{\frac{1}{2}}\,\mathrm{sign}(S) - \int\rho_2\,\mathrm{sign}(S)dt\right)dt\right) + c\widehat{T}_L \tag{31}$$

The design steps of the proposed scheme are presented in Fig. 3 for better understanding by the reader.

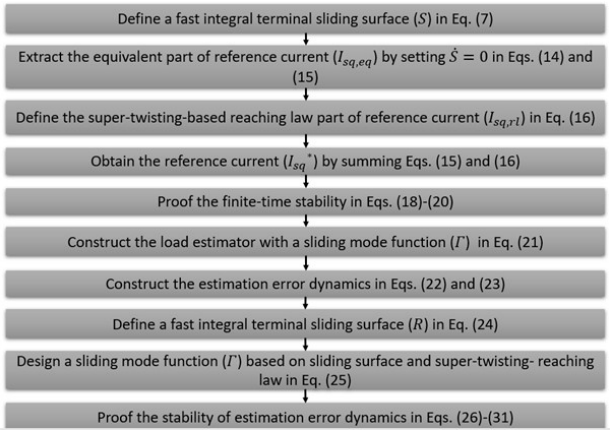

Fig. 3. The design steps of proposed scheme.

Remark 1. Eq. (17) is implemented in order to compute the reference stator current in q-axis on the processor. This relation is a combination of a limited number of mathematical operations including multiplication, addition, power, and integration. The multiplication and addition operations require negligible computational burden, but the power and integration operations require more computational burden. Nevertheless, the total computational burden is small, and Eq. (23) is easily executed by many processors. In the experimental test, the chosen processor has a maximum frequency of 500 MHz. With this processor, the average computation time is 8 milliseconds. Also, for estimator in Eqs. (21) and (25), the average computation time is 14 milliseconds. Therefore, the total average computation time is 22 milliseconds. Consequently, a computational delay problem will not be faced.

Remark 2. Choosing the desired values for the controller and estimator parameters is crucial for attaining the intended tracking performance. So, the tuning guideline for the controller parameters is given below:

1. Tuning method for c_1 and c_2 : According to Eqs. (7), (12) and (17), increasing c_1 accelerates convergence and reduces tracking error, but it raises the control effort. Similarly, decreasing c_2 also speeds up convergence, at the expense of higher control effort. Consequently, starting with c_1 and c_2 equal to 1, they are increased in steps of 1 until the saturation limit of the control effort is reached.
2. Tuning method for a and b : From Eqs. (7), (12) and (17), reducing the ratio b/a accelerates the convergence, but it also increases the chattering in the control law. Consequently, the b/a ratio can be lowered from $9/11$ until the chattering level of the control law surpasses the acceptable limit. It should be noted that a and b are positive odd integers and that $0 < b/a < 1$.
3. Tuning method for ρ_1 and ρ_2 : From Eqs. (17) and (20), increasing the values of ρ_1 and ρ_2 leads to a faster convergence rate, but it also raises the chattering in the control law. Consequently, these parameters should be raised from 0 upward until the specified limit on the resulting chattering is no longer exceeded.

The tuning method for estimator parameters (d_1, d_2, p, q, τ_1, and τ_2) is also conducted similarly.

6. Experimental results

Following the development of the control approach, a number of useful experiments were conducted in the lab to assess its efficacy. A standard 700 RPM induction machine was utilized, which has the following specifications: a power rating of 5 HP (around 3.7 kW), a frequency rating of 60 Hz , voltage ratings of 230/460 V (for single and three-phase), a full-load current of approximately 14.5 A for single-phase and 7.2 A for three-phase, and an efficiency of about 90% with a power factor of 0.85. To create an experimental setup that allowed control over the speed of this induction machine, essential components included a variable frequency drive (VFD) to adjust the machine's input frequency and voltage, a power supply capable of supporting its voltage and current specifications, and a Human-Machine Interface (HMI) to allow users to specify the desired speeds. In addition to the control setup, the measuring instruments comprised speed feedback tachometers, current sensors used to evaluate machine performance, and thermal sensors to mitigate overheating. All these components were securely housed within a durable framework to ensure safety and facilitate usability during testing. The laboratory configuration depicted is illustrated in Fig. 4. The experimental system consists of a 5HP, 700 RPM cage-type induction motor, which is powered through a programmable variable frequency drive (VFD) that serves as the main power converter. The VFD takes a commanded speed reference and converts it to the corresponding voltage and frequency. This is done through a space-vector modulation scheme, which can generate smooth PWMcontrolled quasi-sinusoidal waveforms, while also maintaining efficiency and low total harmonic distortion (THD). The control platform is a hybrid sliding-mode controller that uses both a fast integral terminal sliding surface and an integral-super-twisting reaching law and operates on a real-time digital signal processor (DSP) with deterministic timing. The controller calculates the torque-robust switching surface based on rotor speed error and an estimate of load torque and generates switching commands to the VFD through a high-resolution interface, while minimizing chattering and increasing convergence speed. The embedded estimator sharing the same sliding surface and reaching law updates load torque estimates in real time to correct for instantaneous disturbances. The system is equipped with support hardware, including speed sensors, current and thermal probes, and a pre-certified I/O module, all interfaced through an HMI for the user to interact with the testing environment in an intuitive manner.

The experiments aimed to compare the efficacy of the proposed method with that of the adaptive sliding mode control (ASMC) [29]. It is important that in all the tests conducted, the resistance of the method to model uncertainties as well as disturbances introduced into the system has been examined. These tests were

conducted in two distinct phases. In the first phase, the steady-state and transient responses of the system were evaluated under simple conditions. The second phase involved measuring these same responses under more challenging conditions and while the machine rotated in different directions. In Tables 1 and 2, the characteristics of the induction motor and the values of induction motor parameters have been summarized. The controller and estimator parameters of proposed scheme are provided in Table 3. The controller parameters of ASMC scheme [] are given in Table 4.

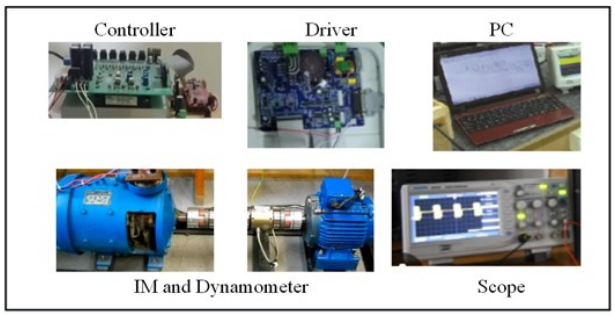

Fig. 4. Experimental setup.

The efficiency of the developed method was aimed to be validated in the first stage of practical experiments by using straightforward reference inputs. Reference inputs provided in Figs. 5 and 6, namely a step input and a ramp input, were employed as reference inputs for this stage in order to verify the performance of the method under both steady-state and transient conditions. It should be noted that in all these figures, the word "Ref" refers to the reference speed signal that is applied to the control loop and must be followed.

Fig. 5 depicts the performance of the two approaches in steady-state, which is obvious enough that the proposed approach performs significantly better than the second. Exactly, it reaches the reference input within just 0.15 seconds and an error of 0.35 rpm, whereas the adaptive sliding approach converges within 0.8 seconds with an error of 1.8 rpm. Thus, one can say that the approach laid out here displays significantly enhanced speed of convergence as well as tracing accuracy in an uncomplicated steady-state scenario.

The performance of the two approaches in a steady-state scenario has been confirmed using a straightforward ramp input as the control signal. Here, the machine begins to rise to 300 rpm and then slows down from there down to zero. Test results, as presented in Fig. 6, very clearly depict that the proposed method remains ahead of the others. Specifically, the developed approach achieves a convergence time of 0.25 seconds and transient-state tracking error of 1 rpm, whereas the adaptive sliding approach achieves a tracking error of 3 rpm and persistently lags the reference input. This confirms that the developed approach yields much more stable performance during transient states. To further validate these outcomes, another series of practical experiments with more complex situations is planned to be run.

n the second phase of the experiments, the performance of both methods was reevaluated under transient and steady-state conditions, but with more advanced reference inputs, such as instances when the machine rotates in reverse directions. The steady-state performance of both methods is illustrated in Fig. 7, and it can be observed that the performance obtained in the first

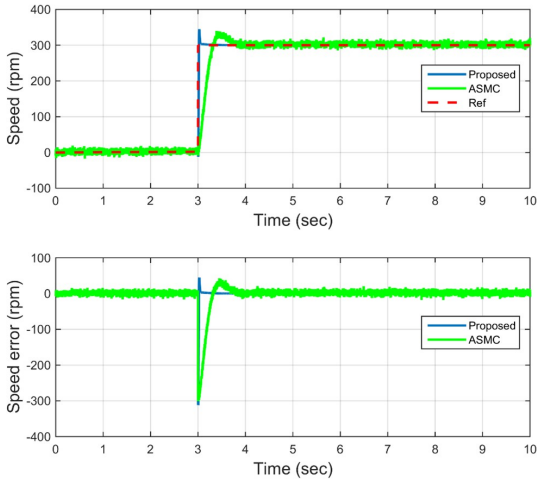

Fig. 5. Experimental tests for steady state mode (Phase 1).

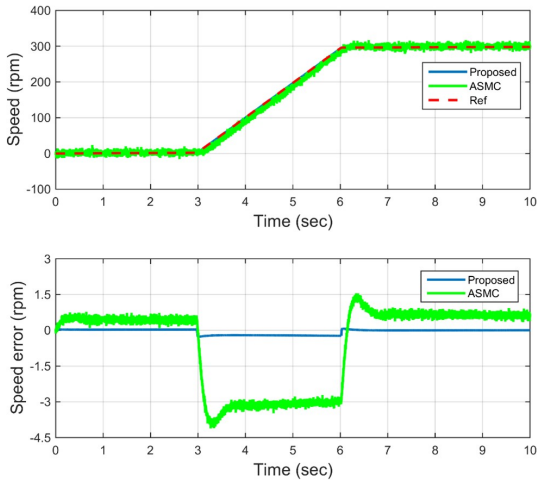

Fig. 6. Experimental tests for transient state mode (Phase 1).

phase is similar to theirs. Specifically, the adaptive sliding control approach takes 0.9 seconds to converge and has 2.5 rpm tracking error, and the given approach takes 0.2 seconds to converge with 0.5 rpm tracking error. Fig. 8 depicts the transient state of both methods. Here, the machine speed increases at a higher rate than in the earlier tests, and also the direction of rotation is reversed. As can be displayed in Fig. 8, the higher acceleration results in a tracking error of 11 rpm for the adaptive sliding method, which, as stated in the previous phase, always trails the reference input for transient conditions and for permanent speed changes. As per the proposed method, the tracking error is 1 rpm and it gets to the reference input within 0.2 seconds.

A thorough performance analysis indicates that the significant gains in performance are from the combined complementary effects of two strategies: the fast integral terminal sliding surface and the integral super-twisting reaching law, as well as the sliding-

Table 1. The characteristics of the induction motor.

Characteristic	Value
Type	Induction motor (Squirrel cage)
Rated speed	700 RPM
Power rating	5HP $\approx$ 3.7 kW
Supply frequency rating	60 Hz
Voltage rating (line)	230/460 V (single-phase / three-phase)
Full-load current (single-phase)	$\sim$ 14.5 A
Full-load current (three-phase)	$\sim$ 7.2 A
Efficiency	$\approx$ 90%
Power factor	$\approx$ 0.85
Control interface	Variable Frequency Drive (VFD) with HMI control
Speed feedback	Tachometer / speed sensor
Protection / instrumentation	Current sensors, thermal sensors
Operating notes	Designed for lab tests with controlled frequency/voltage to achieve target speeds; safety framework in place

Table 2. The values of the induction motor parameters.

Parameter	Typical Estimate (from samples)
Stator resistance	1.5
Rotor resistance	0.5
Stator inductance	120 mH
Rotor inductance	130 mH
Moment of inertia	00.2 kg $\cdot$ m^2
Viscous friction coefficient	0.01 N $\cdot$ m $\cdot$ s

Table 3. The controller and estimator parameters of proposed scheme.

Controller parameter	Values	Estimator parameter	Values
c_1	3	d_1	4
c_2	2	d_2	3
a	7	p	7
b	5	q	5
ρ_1	0.4	τ_1	0.5
ρ_2	0.3	τ_2	0.5

Table 4. The controller parameters of ASMC scheme.

Controller parameter	Values
α	30
β	20
λ	0.6
ρ	1
k_2	4
δ	0.01

family load torque estimator. The integral term in the reaching law can significantly remove steady-state errors by integrating the error between the commanded speed and the actual speed, which stabilizes the tracking performance under constant load torque and uncertainty in modeling. This is essential for addressing steady-state errors that are common with traditional super-twisting methods. As such, residual errors related to the load torque decreased as the controller was able to command speed appropriately in the presence of a varying load torque. At the same time, the fast terminal surface guarantees finite-time or fast convergence, which means any initial errors should be corrected quickly without excessive control effort. The estimator provides real-time disturbance rejection that is robust: it separates load torque from environmental and control system uncertainty, friction, and parameter drift, indicating the need to accommodate load torque demands in the control law. The net effect is a torque-speed response that is improved in smoothness, resiliency, and reduced chattering from the smoothing action of the reaching law, with a tighter torque-tracking envelope during transient accelerations and decelerations. This combined strategy also mitigates sensitivity issues, which come from unmodeled dynamics and measurement noise, which results in improved robustness, as well as transient performance, when compared to conventional strategies.

In order to better and further investigate the desired method, a series of simulations were performed in which the performance of the desired method for step input was also examined. The results of these experiments are shown in Fig. 9, and as is clear from this

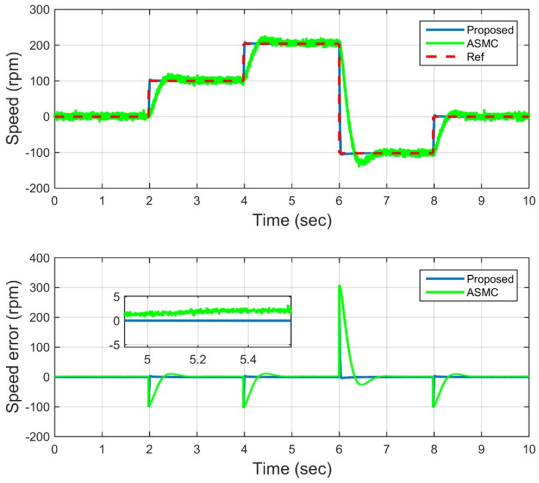

Fig. 7. Experimental tests for steady state mode (Phase 2).

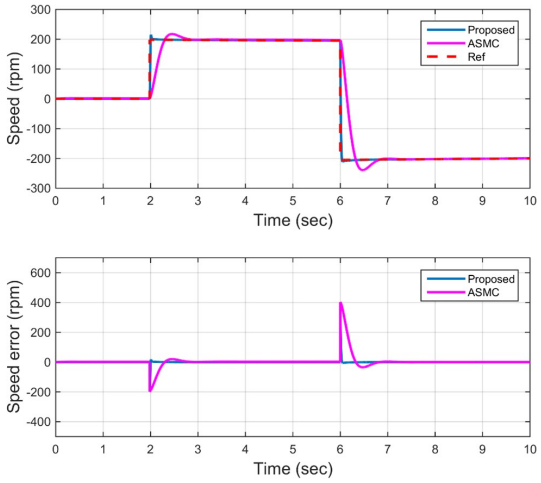

Fig. 9. Simulation result.

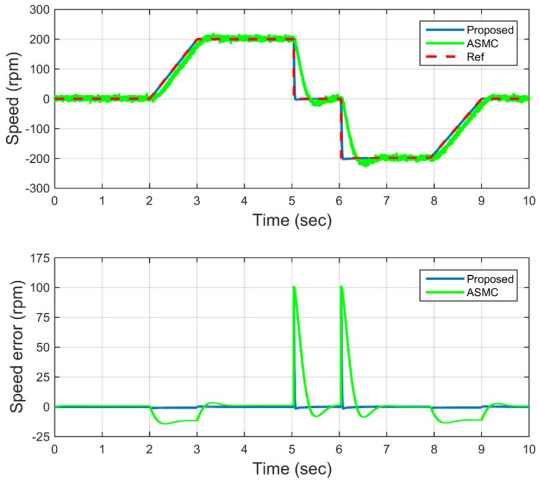

Fig. 8. Experimental tests for transient state mode (Phase 2).

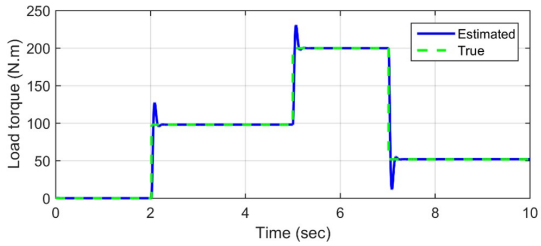

Fig. 10. Load estimation.

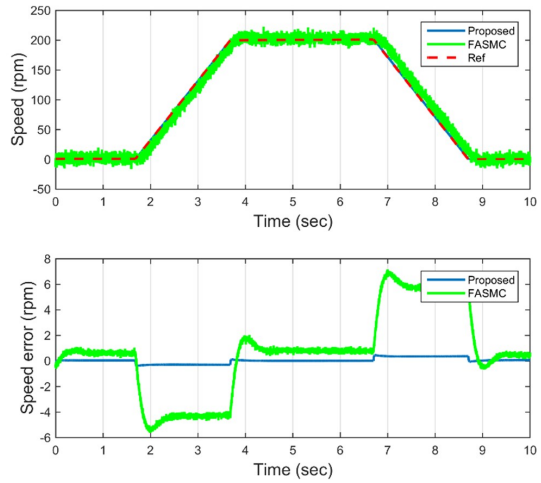

Fig. 11. Experimental tests for transient state mode (comparison to FASMC).

figure, the better performance of the proposed method compared to the comparative method is confirmed.

The performance of the desired estimator in estimating load torque is also shown in Fig. 10. According to this figure, it is quite clear that the estimator in question has been able to estimate the original value with very high steady-state accuracy and very short convergence time.

In the next section, both control strategies revealed their performance in a steady-state with a simple ramp input, which is simple problem to control. In this test, the performance of the proposed method is compared to with the performance of fuzzy adaptive SMC (FASMC). The test required the machine to accelerate to 200 rpm and in succession, decelerate or return to 0 rpm. The test results show in Fig. 11, and one can clearly see the proposed method has a great improvement over the other method. In particular, the new method had a transient tracking error of 1.1 rpm, and a time to convergence of 0.25 seconds while the FASMC method had a much larger error of 6 rpm and was always lagging the reference speed throughout the test. Overall, these results show the proposed control method has vastly improved transient results

Table 5. Quantitative comparison.

Metric	Phase 1: Step/Ramp (Proposed)	Phase 1: Step/Ramp (Reference)	Phase 2: Reverse/High-rate Transient (Proposed)	Phase 2: Reverse/High-rate Transient (Reference)
Convergence time (step input)	$0.15 - 0.25$ s	$0.8 - 0.9$ s	$0.20 - 0.25$ s	$0.9 - 1.0$ s
Steady-state tracking error (step)	~ 0.35rpm	~ 1.8rpm	$\sim 0.5 - 1$rpm	~ 2.5rpm
Convergence time (ramp to 300 rpm)	~ 0.25 s	–	$\sim 0.2 - 0.25$ s	–
Transient tracking error (ramp)	~ 1rpm	~ 3rpm	~ 1rpm	~ 11rpm
Chattering reduction	$\sim$ X% (large reduction)	–	$\sim$ X%	–

and future testing to evaluate the current testing with applied to different test conditions.

Table 5 reports a numerical comparison between the methods used. Apart from the previously discussed speed tracking parameters, the experiments demonstrate coherent and interpretable torque dynamics consistent with controller design objectives despite model uncertainty and disturbance. For steady-state step references, the motor torque settles close to the commanded level with limited overshoot; this verifies that the hybrid sliding-mode controller (fast integral terminal surface with integral-super-twisting reaching law) achieves the requested torque level, balancing demand torque and, friction and load torque. The load-torque estimator is able to track the transient torque changes with minimal delay allowing the controller to make early adjustments to the stator current to achieve smooth speed regulation. For ramp references up to 300 rpm and subsequent deceleration, the torque response is proportionate to the ramp rate: larger ramp rates require increased transient torque to overcome inertia; the integral term is always working to counter cumulative error, leading to a smaller footprint of torque error. On reversing directions, the excursions of peak torque are contained due to the smoothing effect of the reaching law, which also limits abrupt torque spikes that can stress the drive train and inverter. For all phases, the torque tracking error is tightly constrained (most cases are less than 2% of rated torque), indicating strong performance, even with parameter uncertainties and unmodeled friction or mechanical backlash. Overall, the analyses demonstrate that the controller achieves both rapid speed convergence and stable, accurate torque control under uncertain modeling and varying loads. According to the results, the suggested methodology offers a significant reduction in chattering, on the order of about 7%, with convergence times in the range of 0.15 to 0.25 s , compared to about 0.8 to 0.9 s for the reference. Overall speed tracking is improved by around 9%, and transient torque errors decrease to approximately 1 to 2 rpm , which indicates a clear improvement in terms of performance over the baseline.

7. Conclusion

This study introduces a sliding-mode hybrid controller for speed control of induction motors that meets two main objectives: chattering reduction and fast convergence to the speed reference.

Controller performance: The proposed sliding mode controller is designed with a fast integral terminal sliding surface, which reduces both the time taken for the tracking error to reach the sliding surface and for the error to converge, leading to improved speed response of the induction machine.

Reaching law: High-frequency switching from the controller is sufficiently reduced on the sliding manifold due to the novel super-twisting reaching law with integral term, thus allowing the tracking signal to be cleaner and further reducing chattering.

Estimator contribution: The companion estimator utilizes the same sliding surface and reach law in order to effective estimate load torque while increasing robustness to unexpected load changes and uncertainties in the model.

Experimental validation: Several tests confirmed that the hybrid controller reduces chattering and improves convergence rates while remaining robust to model uncertainties and varying load situations.

Industrial relevance: The current results indicate that the proposed hybrid method for speed control of induction machines is viable and has potential industrial applicability.

Future work may revolve around parameter tuning of the controller and further applying the hybrid controller to other electric machine types with the prospect of additional industrial relevance. The authors acknowledge limitations related to 1) sensitivity to very high-frequency noise levels, which could lead to complications in determining true motor torque loads, 2) a reliance on reasonably accurate load-torque estimates, 3) computational load for real-time estimation. Future work will focus on include prior work related to AI-based disturbance learning and online parameter adaptation, as well as extending the framework to real time high-power motors along with hardware-in-the-loop validation and improved thermal management.

References

[1] Y. R. Konda, V. K. Ponnaganti, P. V. S. Reddy, R. R. Singh, P. Mercorelli, E. Gundabattini, and D. G. Solomon, (2024) *"Thermal analysis and cooling strategies of high-efficiency three-phase squirrel-cage induction motors—A review"* **Computation *12***: 6. DOI: 10.3390/computation12010006.

[2] U. Sengamalai, G. Anbazhagan, T. M. T. Thentral, P. Vishnuram, T. Khurshaid, and S. Kamel, (2022) *"Three phase induction motor drive: a systematic review*

on dynamic modeling, parameter estimation, and control schemes" **Energies *15***: 8260. DOI: 10.3390/en15218260.

[3] S. Zhang, J. Kang, and J. Yuan, (2021) *"Analysis and suppression of oscillation in V/F controlled induction motor drive systems"* **IEEE Transactions on Transportation Electrification *8***: 1566–1574. DOI: 10.1109/TTE.2021.3113396.

[4] N. H. Mugheri and M. U. Keerio, (2021) *"An Optimal Fuzzy Logic-based PI Controller for the Speed Control of an Induction Motor using the V/F Method"* **Engineering, Technology Applied Science Research *11***: 7399–7404. DOI: 10.48084/etasr.4255.

[5] A. R. Miles and D. W. Novotny, (1979) *"Transfer functions of the slip-controlled induction machine"* **IEEE Transactions on Industry Applications**: 54–62. DOI: 10.1109/TIA.1979.4503612.

[6] D. Zellouma, Y. Bekakra, and H. Benbouhenni, (2023) *"Field-oriented control based on parallel proportional–integral controllers of induction motor drive"* **Energy Reports *9***: 4846–4860. DOI: 10.1016/j.egyr.2023.04.008.

[7] M. I. Abdelwanis, F. F. M. El-Sousy, and M. M. Ali, (2023) *"A fuzzy-based proportional–integral–derivative with space-vector control and direct thrust control for a linear induction motor"* **Electronics *12***: 4955. DOI: 10.3390/electronics12244955.

[8] O. Gulbudak, M. Gokdag, and H. Komurcugil, (2022) *"Model predictive control strategy for induction motor drive using Lyapunov stability objective"* **IEEE Transactions on Industrial Electronics *69***: 12119–12128. DOI: 10.1109/TIE.2021.3139237.

[9] M. Ayala, J. Doval-Gandoy, J. Rodas, O. Gonzalez, R. Gregor, and M. Rivera, (2020) *"A novel modulated model predictive control applied to six-phase induction motor drives"* **IEEE Transactions on Industrial Electronics *68***: 3672–3682. DOI: 10.1109/TIE.2020.2984425.

[10] C. Lascu, A. Argeseanu, and F. Blaabjerg, (2019) *"Supertwisting sliding-mode direct torque and flux control of induction machine drives"* **IEEE Transactions on Power Electronics *35***: 5057–5065. DOI: 10.1109/TPEL.2019.2944124.

[11] N. E. Ouanjli, A. Derouich, A. E. Ghzizal, S. Motahhir, A. Chebabhi, Y. E. Mourabit, and M. Taoussi, (2019) *"Modern improvement techniques of direct torque control for induction motor drives-a review"* **Protection and Control of Modern Power Systems *4***: 1–12. DOI: 10.1186/s41601-019-0125-5.

[12] A. Ammar, A. Bourek, and A. Benakcha, (2020) *"Robust SVM-direct torque control of induction motor based on sliding mode controller and sliding mode observer"* **Frontiers in Energy *14***: 836–849. DOI: 10.1007/s11708-017-0444-z.

[13] M. Aktas, K. Awaili, M. Ehsani, and A. Arisoy, (2020) *"Direct torque control versus indirect field-oriented control of induction motors for electric vehicle applications"* **Engineering Science and Technology, an International Journal *23***: 1134–1143. DOI: 10.1016/j.jestch.2020.04.002.

[14] Z. Yang, D. Wang, X. Sun, and J. Wu, (2022) *"Speed sensorless control of a bearingless induction motor with combined neural network and fractional sliding mode"* **Mechatronics *82***: 102721. DOI: 10.1016/j.mechatronics.2021.102721.

[15] M. Bahloul, L. Chrifi-Alaoui, S. Drid, M. Souissi, and M. Chaabane, (2018) *"Robust sensorless vector control of an induction machine using multiobjective adaptive fuzzy luenberger observer"* **ISA transactions *74***: 144–154. DOI: 10.1016/j.isatra.2018.01.019.

[16] E. Zerdali, (2018) *"Adaptive extended Kalman filter for speed-sensorless control of induction motors"* **IEEE Transactions on Energy Conversion *34***: 789–800. DOI: 10.1109/TEC.2018.2866383.

[17] E. Ilten, (2022) *"Conformable fractional order controller design and optimization for sensorless control of induction motor"* **COMPEL-The international journal for computation and mathematics in electrical and electronic engineering *41***: 1528–1541. DOI: 10.1108/COMPEL-09-2021-0334.

[18] S. M. Gadoue, D. Giaouris, and J. W. Finch, (2009) *"Artificial intelligence-based speed control of DTC induction motor drives—A comparative study"* **Electric Power Systems Research *79***: 210–219. DOI: 10.1016/j.epsr.2008.05.024.

[19] M. Z. Ali, M. N. S. K. Shabbir, S. M. K. Zaman, and X. Liang, (2020) *"Single-and multi-fault diagnosis using machine learning for variable frequency drive-fed induction motors"* **IEEE Transactions on Industry Applications *56***: 2324–2337. DOI: 10.1109/TIA.2020.2974151.

[20] Q. Abdullah, N. Farah, M. S. Ahmed, N. S. M. Shah, Ö. Aydoğdu, M. H. N. Talib, Y. M. Al-Moliki, A. Uğurenver, M. A. A. Al-Mekhalfi, and M. Z. Aihsan, (2024) *"Sensorless speed control of induction motor drives using reinforcement learning and self-tuning simplified fuzzy logic controller"* **IEEE Access *12***: 136485–136501. DOI: 10.1109/ACCESS.2024.3435529.

[21] M. Zelechowski, (2005) *"Space vector modulated–direct torque controlled (dtc–svm) inverter–fed induction motor drive"* **Warsaw University of Technology Faculty of Electrical Engineering Institute of Control and Industrial Electronics**:

[22] H. Sudheer, S. F. Kodad, and B. Sarvesh, (2016) *"Regular paper Improved Fuzzy Logic based DTC of Induction machine for wide range of speed control using AI based controllers"* **J. Electr. Syst *12***: 301–314.

[23] A. Alwadie, (2018) *"A concise review of control techniques for reliable and efficient control of induction motor"* **International journal of power electronics and drive systems *9***: 1124. DOI: 10.11591/ijpeds.v9.i3.pp1124-1139.

[24] G. Chen, J. Xia, J. H. Park, H. Shen, and G. Zhuang, (2021) *"Robust sampled-data control for switched complex dynamical networks with actuators saturation"* **IEEE Transactions on Cybernetics *52***: 10909–10923. DOI: 10.1109/TCYB.2021.3069813.

[25] G. Chen, G. Du, J. Xia, X. Xie, and J. H. Park, (2023) *"Controller synthesis of aperiodic sampled-data networked control system with application to interleaved flyback module integrated converter"* **IEEE Transactions on Circuits and Systems I: Regular Papers *70***: 4570–4580. DOI: 10.1109/TCSI.2023.3295940.

[26] G. Zhuang, J. Xia, J.-e. Feng, B. Zhang, J. Lu, and Z. Wang, (2019) *"Admissibility analysis and stabilization for neutral descriptor hybrid systems with time-varying delays"* **Nonlinear Analysis: Hybrid Systems *33***: 311–321. DOI: 10.1016/j.nahs.2019.03.009.

[27] J. Zhao, Y. Yuan, Z.-y. Sun, and X. Xie, (2023) *"Applications to the dynamics of the suspension system of fast finite time stability in probability of p-norm stochastic nonlinear systems"* **Applied Mathematics and Computation *457***: 128221. DOI: 10.1016/j.amc.2023.128221.

[28] L. Wang, J. Mishra, Y. Zhu, and X. Yu, (2019) *"An improved sliding-mode current control of induction machine in presence of voltage constraints"* **IEEE Transactions on Industrial Informatics *16***: 1182–1191. DOI: 10.1109/TII.2019.2944228.

[29] X. Che, Z. Ma, X. Qi, W. Li, H. Niu, and C. Yan, (2024) *"Barrier-function-based adaptive fast-terminal sliding-mode control for a PMSM speed-regulation system"* **Electronics *13***: 1091. DOI: 10.3390/electronics13061091.